

Multi-Level Logic Gate Operation Based on Amplified Aptasensor Performance**

Lingyan Feng, Zhaozi Lyu, Andreas Offenhäusser, and Dirk Mayer*

Abstract: Conventional electronic circuits can perform multi-level logic operations; however, this capability is rarely realized by biological logic gates. In addition, the question of how to close the gap between biomolecular computation and silicon-based electrical circuitry is still a key issue in the bioelectronics field. Here we explore a novel split aptamer-based multi-level logic gate built from INHIBIT and AND gates that performs a net XOR analysis, with electrochemical signal as output. Based on the aptamer–target interaction and a novel concept of electrochemical rectification, a relayed charge transfer occurs upon target binding between aptamer-linked redox probes and solution-phase probes, which amplifies the sensor signal and facilitates a straightforward and reliable diagnosis. This work reveals a new route for the design of bioelectronic logic circuits that can realize multi-level logic operation, which has the potential to simplify an otherwise complex diagnosis to a “yes” or “no” decision.

A wide and diverse range of DNA molecular devices have been realized in the past decade with the goal of harnessing specific properties of molecules as electric components for molecular-scale computing.^[1] Various Boolean logic operations have been developed with different applications in biology, ranging from biosensors to bioimaging and therapeutics, which primarily focus on the basic logic functions, AND, OR, and XOR.^[2] For integrated electronic circuits, a multi-level logic operation can be easily performed by wiring different logic gates together electrically. However, the connection of biological logic gates to form a multi-level circuit poses significant challenges. Although enzymatic networks with hierarchical circuit design,^[3] as well as modular DNA-based Boolean logic gates wired into a three-level circuit have been reported that exhibited a Boolean XOR function,^[4] most logic gates (mainly DNA-based) employ fluorescent or colorimetric signals as their outputs. These optical signals prove cumbersome for further linking of different logic gates and their integration with electronic devices. In order to design multi-level logic gates and further

close the gap between DNA computation and electrical circuitries, the future of such logic elements is closely related to the successful linkage of nucleic acid to a conductive or semiconductive support with electrochemical (electric) signals as their outputs, as well as functional DNA recognition motifs to implement special biological applications. Just a few pioneering attempts have been performed to immobilize DNA logic gates on electrochemical supports, however, with only one- or two-level logic operations.^[5]

Recently, a novel kind of molecular recognition element has been developed that is based on specific single-strand DNA/RNA molecules selected from libraries with random sequences.^[6] The so-called aptamers offer great flexibility in terms of structure variants to bind to a variety of targets with high affinity and specificity, and are promising candidates for bioanalytical applications and new computing systems.^[7] Moreover, when a single aptamer splits into two fragments, they usually can form associated sandwich-type complexes with their target.^[8] Herein we extend this concept of a split aptamer-based electrochemical sensor by incorporating a novel electronic element, namely electrochemical current rectification (ECR) for signal amplification capabilities and its application in multi-level logic circuits.

Interest in ECR has increased rapidly due to its ability to facilitate unidirectional current flow across an electrochemical interface.^[9] A characteristic property of the ECR process reported here is that the entire charge transfer occurs only in one direction between solution-phase redox probes and electrode via surface-confined redox groups. It has been successfully implemented in bioelectronic and bioelectrochemical systems through the incorporation and tailoring of biomolecules into supramolecular bioassemblies to perform electronic operations.^[10] Furthermore, our group recently reported the application of ECR for mimicking molecular logic gate operations, as well as the realization of transistor functions with signal amplification.^[11]

We set out to design a multi-level aptamer-based logic gate, which is built from sequential INHIBIT (INH) and AND gates, that performs a net XOR analysis, with electrochemical signal as output. We used ATP and its split aptamers as a model; one INH logic gate is initially constructed as the starting point of the logic operation (Figure 1 A). The 27-mer ATP aptamer is divided into two parts with different sequences.^[8,12] First, the electrode surface is modified by a 14-mer split aptamer (Apt-1) through covalent thiol–gold bonds (Figure 1 B, curve a). When the second 13-mer split aptamer strand (Apt-2) bearing a ferrocene (Fc) tag is applied, a stable sandwiched structure forms through target–ATP binding. An anodic peak at around 0.35 V and a cathodic peak at around 0.28 V (vs. Ag/AgCl) can be

[*] Dr. L. Feng, Z. Lyu, Prof. A. Offenhäusser, Dr. D. Mayer
Peter Grünberg Institute, PGI-8, Research Center Jülich
JARA – Fundamentals of Future Information Technology
Jülich 52425 (Germany)
E-mail: dirk.mayer@fz-juelich.de

[**] We thank Dr. Youlia Mourzina for helpful comments on the manuscript and the Federal Ministry of Education and Research (Germany), funding code 031A095B. Dr. L. Feng also thanks the Alexander von Humboldt Foundation for a Humboldt fellowship.



Supporting information for this article is available on the WWW under <http://dx.doi.org/10.1002/anie.201502315>.

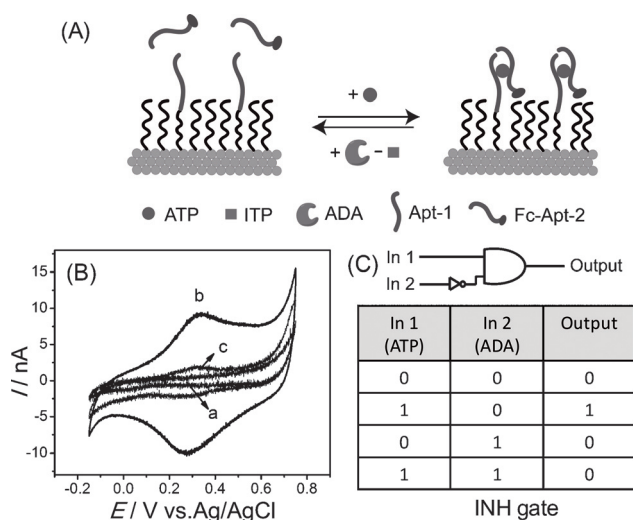


Figure 1. A) Schematic illustration of the ATP split aptamer-based INH logic gate. In the presence of ATP, a sandwich complex is formed between the surface-tethered split aptamer (Apt-1) and the ferrocene-containing split aptamer (Apt-2). ADA is able to catalyze the conversion of ATP to inosine triphosphate (ITP). The latter shows no interaction with the ATP aptamer and the sandwich aptamer complex dissociates. B) CV curves of different electrode surfaces: a) Apt-1-modified gold electrode; b) Apt-1-modified electrode after incubation in $1 \mu\text{M}$ Apt-2 solution in the presence of $500 \mu\text{M}$ ATP and c) in the presence of both ATP and 0.1 U mL^{-1} ADA. C) The INH logic scheme and truth table.

measured (Figure 1B, curve c). The system responds quite differently in the absence of ATP molecules due to the thermal instability of target-free aptamer complex.^[13] The peak position and the equal peak heights clearly indicate a reversible and surface-confined electron transfer between Fc and the electrode (Figure S1). Under optimized modification conditions (Figures S2 and S3), the DNA surface density is calculated to be about $(3.85 \pm 0.33) \times 10^{11} \text{ molecules cm}^{-2}$, which corresponds to previously reported DNA densities.^[14] Beyond that, an ATP-aptamer complex that has already been formed can be dissociated by applying adenosine deaminase (ADA) (Figure 1B, curve c). ADA is a key hydrolytic enzyme in purine metabolism that can efficiently catalyze the deamination of adenosine (deoxyadenosine) into inosine (deoxyinosine), for which the ATP aptamer shows no detectable affinity. This makes it possible for ADA to break the formed sandwich structure.^[15] Inherited ADA deficiency is one main cause for severe combined immune deficiency disease (SCID).^[16] In contrast, ADA plethora may also cause diseases, such as tuberculosis and hemolytic anemia.^[17] In healthy human plasma the ATP concentration is roughly on the μM level, and the ADA activity is on the level of 0.03 U mL^{-1} .^[18] Too high or too low ATP/ADA concentrations are critically harmful for human beings. Our present logic gate is expected not only to link multi-level logic gates

together, but also to supply diagnostic information on a coupled biological system.

To produce an INH logic gate, high levels of ATP (In1) and ADA (In2) are defined at $\geq 10 \mu\text{M}$ and at $\geq 0.03 \text{ U mL}^{-1}$, respectively, as the “1” states while lower concentrations of each of these are defined as the “0” states. For the output of the INH gate, the electrochemical signal in the presence of $10 \mu\text{M}$ ATP represents the threshold. If the current value is higher than this, it is considered as “1”, while lower values are considered as “0”. In evaluating the four different states in the presence and/or absence of ATP and ADA, namely (0,0) (1,0) (0,1) (1,1), only (1,0) induces a significant relative current change, resulting in a “1” output. Thus, an INH operation can be realized by controlling the concentrations of the ATP and ADA activity unit (Figure 1C and Figure S4).

One important concern about such a design is that the signal obtained by this method is strongly dependent on the surface probe density, which is typically in the range of a few pmol cm^{-2} or even less. The low probe density usually affects the platform’s sensitivity and applicability.^[14] Therefore we introduce the concept of electrochemical rectification (ECR) for signal amplification.

Starting from the outputs of the INH gate, a third input, ferrocyanide (In3), is then introduced into the system to perform the second-level logic operation. The ECR effect is realized through a relayed charge transport between split aptamer-linked Fc groups and solution-phase redox probes as shown in Figure 2A. Due to their different redox potentials, the charge transfer can be efficiently relayed from the

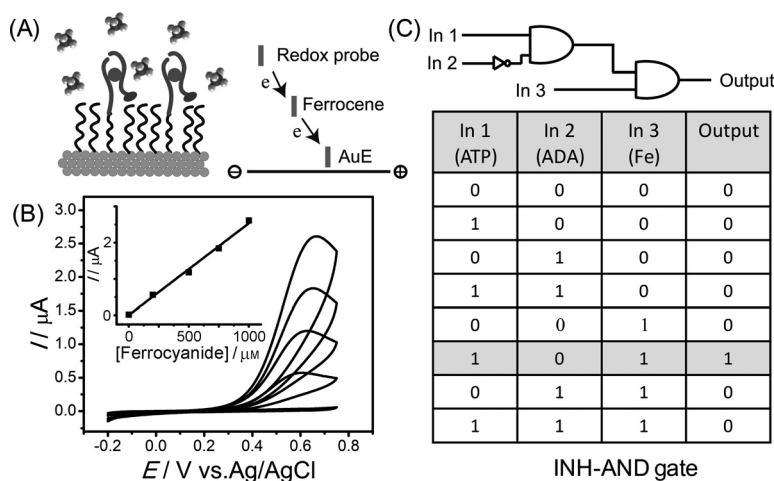


Figure 2. A) Electrochemical current rectification (ECR) scheme. The ECR effect is realized through a relayed charge transport between the split aptamer-linked Fc tag and the solution-phase redox probes. B) CV curves in $\text{K}_4[\text{Fe}(\text{CN})_6]$ solutions of different concentrations. Inset: the linear relationship between peak current and $\text{K}_4[\text{Fe}(\text{CN})_6]$ concentration. C) The two-level INH-AND logic scheme and truth table.

electrode via the Fc center (Fc⁺/Fc redox potential around $0.32 \text{ V vs. Ag/AgCl}$) to ferrocyanide (Fe³⁺/Fe²⁺ redox potential $0.21 \text{ V vs. Ag/AgCl}$), which leads to a significant increase in the anodic current (Figure 2A). In the reverse direction, however, the electron-transfer process is thermodynamically forbidden.^[11,19] The surrounding of the surface-tethered

aptamer strand was backfilled with insulating 1-undecanethiol molecules to eliminate the direct charge transfer between the electrode and the solution-phase redox probes via defects in the self-assembled monolayer (Figure S5).^[19] The height of the sensor signal can be easily amplified by tuning the concentration of electron-donating redox probes in the solution (Figure 2B). The solution-phase redox probes diffuse to the electrode to continuously replenish electrons to the charge-transfer mediator and thus amplify the current response with a linear relationship (Figure 2B, inset). A concentration of 1 mM is selected for the solution-phase redox probes in the following sections (Figures S6 and S7). The whole rectified current (j) can be tuned through two adjustable chemical parameters [Eq. (1)]: the concentration of the redox probes in solution as discussed above, and the population of redox sites on the electrode introduced by target binding and the formation of the aptamer sandwich structure (Figure 2A).^[10]

$$j = F\kappa_{\text{cross}}\Gamma_0 c_{\text{D}} \quad (1)$$

Equation (1) includes the Faraday constant F and the rate constant κ_{cross} for the reaction between surface-confined Fc groups and the solution-phase redox probe. Γ_0 is the coverage of redox-active sites on the surface, and c_{D} is the concentration of the solution-phase donor (or acceptor) probe. The number of surface redox sites on the electrode depends exclusively on the amount of Fc-labeled Apt-2 aptamer in the presence of ATP. The relationship between the amplified peak current and the ATP target concentrations was determined, and it exhibited a sensitive response for the target with a detection limit of about 7.5 nM (Figure 3A; Figure S8). This result represents an improvement of around 130 times compared with the detection limit of 1 μM achieved in the absence of ECR-based amplification (Figure S9). The aptasensor selectivity was proven through a comparison with other target analogues and a direct detection in complicated serum solutions (Figure S10). Based on the same mechanism, this aptasensor is also sensitive to ADA activity response, since Fc-linked Apt-2 is released from the surface after enzyme treatment (Figure S11). An ADA activity detection as low as 0.002 U mL^{-1} can be obtained with a higher sensitivity and an excellent selectivity compared with previously reports (Figure 3B, Figure S12, and Table S1).

Neither the detection of ATP nor ADA activity is affected by the presence of interfering compounds in complex media. Furthermore, the magnification of signal induced by ATP binding occurs without the permeation of the mixed self-assembled monolayer by solution-phase probes. This is an important advantage of ECR-based amplification compared with previously reported electrocatalytic amplification principles, since a permeation reaction would reduce the charge-transfer efficacy between surface-confined probe and solution-phase probe.^[20] Our simple ECR amplification scheme does not rely on comparatively expensive enzymes, stringent environmental conditions, or complicated synthesis processes.^[21] Therefore it can be concluded that the concept of ECR-based signal amplification provides a suitable and more

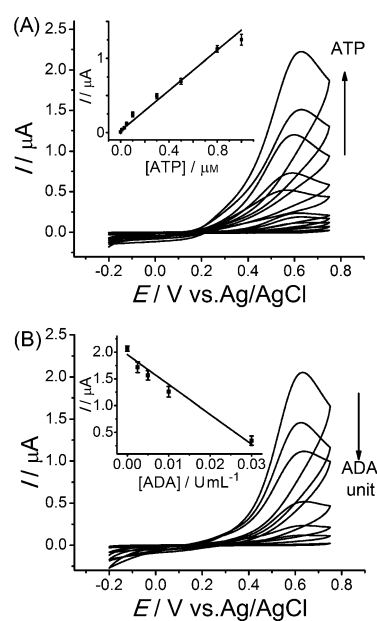


Figure 3. A) CV curves with amplified anodic currents caused by increasing ATP concentrations from 0.01 to 50 μM , in the presence of 1 mM $\text{K}_4[\text{Fe}(\text{CN})_6]$. Inset: Enlargement of the linear region at low ATP concentrations. B) CVs recorded from an as-prepared electrode with the surface-tethered ATP/aptamer complex during ADA activity detection with different activity units (0, 0.0025, 0.005, 0.01, 0.03, 0.05, 0.1) U mL^{-1} . Inset: Linear region of peak current and ADA activity unit.

general tool for the enhancement of aptamer-based biosensor performance.

However, the additional third input (In3) not only enables signal amplification but also introduces a second-level logic gate, which facilitates distinguishable output signals by raising the output threshold values. Therefore, the output of the INH logic gate described above and In3 can be considered as inputs to enter into the next INH-AND logic operation, with logic scheme and corresponding truth table shown in Figure 2C. Noteworthy, here we defined different threshold values for the final output current produced by the split aptamer-based electrode due to ECR-based signal amplification. The region with an absolute current value higher than 1.5 μA (when $\text{ATP} \geq 10 \mu\text{M}$ or $\text{ADA} < 0.01 \text{U mL}^{-1}$) was defined as “1”, and the second region with a current value lower than 0.1 μA (when $\text{ATP} < 0.1 \mu\text{M}$ or $\text{ADA} \geq 0.03 \text{U mL}^{-1}$) was defined as “0”, with a difference of a factor of 15 between them to avoid ambiguous states (Figure 3). This gray region between “1” and “0”, which lacks any definite response, corresponds to the usual amount of ATP (0.1 to 10 μM) and ADA activity unit (0.01 to 0.03 U mL^{-1}) in normal human serum.^[18] This definition is also analogous to the approach used in electronics where only appropriate voltage regions are employed to define the logic functions. With the help of ECR, the different sensor responses to ATP concentration and ADA activity are much easier to analyze and the logic gate directly indicates different states of health. The current increases significantly only when $\text{In1} = 1$ ($\text{ATP} \geq 10 \mu\text{M}$), $\text{In2} = 0$ ($\text{ADA} < 0.01 \text{U mL}^{-1}$), and $\text{In3} = 1$ (1 mM ferrocyanide), yielding

a “1” output in the presence of solution-phase probes for ECR-aided signal amplification. This usually indicates a disease status, for instance, the presence of a severe combined immunodeficiency.^[22] Otherwise, the current intensity is lower which corresponds to an output signal “0” (Figure 2 C and Figure S13). According to the clinical studies,^[18b] patients with tuberculosis usually have higher levels of ADA activity ($\text{ADA} \geq 0.03 \text{ U mL}^{-1}$) in their serum, which corresponds to inputs (0,1,1) or (1,1,1). Both of the output signals, “0” and “1”, supply diagnosis information that indicate a physical impairment. Only if the inputs are within the gray range is the diagnosis without findings.

Based on these amplified aptasensor performances with the ECR effect, we continue to construct a multi-level logic gate and combine the INH–AND gate with an XOR function (Figure 4 A). Instead of an anodic rectification based on

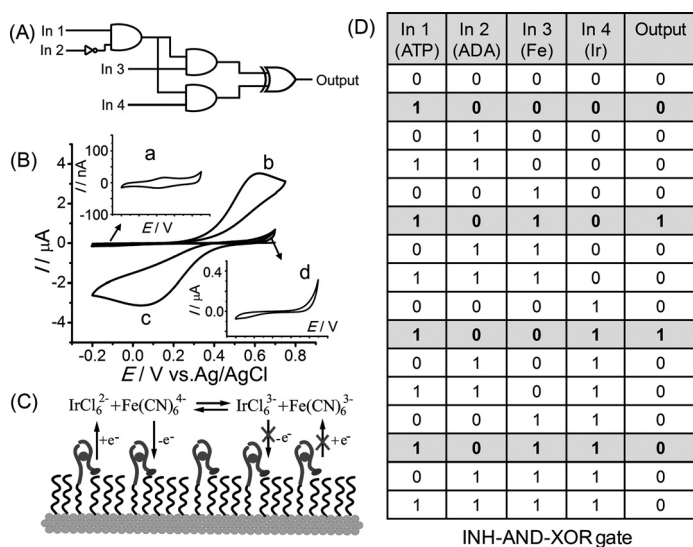


Figure 4. A) The INH–AND–XOR logic scheme built from INHIBIT and AND gates that performs a net XOR analysis. B) The as-prepared split aptamer sensor in the presence of different inputs: a (1,0,0,0), b (1,0,1,0), c (1,0,0,1), and d (1,0,1,1). The anodic and cathodic current amplification are realized with 1 mM $\text{K}_4[\text{Fe}(\text{CN})_6]$ and 1 mM K_2IrCl_6 , respectively, in the same range of CV potentials. C) Schematic illustration of the electron-transfer processes between redox species and the aptamer-modified electrode surface. The chemical equation demonstrates the direct charge transfer between the two redox probes in solution. D) Truth table of the multi-level logic gate designed for this work.

ferrocyanide, the cathodic current can also be amplified simply by changing the solution redox species from ferrocyanide (0.21 V vs. Ag/AgCl) to hexachloriridate(IV) (0.68 V vs. Ag/AgCl). The different redox potentials of the solution-phase redox probes lead to different directions of the charge transfer between the surface-bound Fc center (Fc^+/Fc redox potential 0.32 V vs. Ag/AgCl) and electron-donating (ferrocyanide, $\text{Fe}^{3+}/\text{Fe}^{2+}$)/electron-accepting (hexachloriridate, $\text{Ir}^{4+}/\text{Ir}^{3+}$) species in solution (Figure 4 B). In 3 and In 4 correspond to the addition of 1 mM ferrocyanide and iridate(IV) ions, respectively, while the absence of the respective species is considered to constitute “0”. With the same output definition

as discussed above in the INH–AND logic gate, three regions of “1”, “0”, and “gray” are adopted for the intensity of output signals. A three-level logic function can be realized by adjusting different input values. When only one type of redox probe is added to the solution, the aptamer-modified electrode can be considered as an anodic or cathodic ECR. This ECR functions similar to a diode, which facilitates an electric current in one direction (forward-biased conditions) and blocks the current in the opposite direction (reverse-biased conditions), resulting in an INH–AND logic gate (Figure 4 B, curves b and c). When both In 3 and In 4 are applied simultaneously, the current responses decrease largely because of the interplay of different interfacial and solution-based charge-transfer processes (Figure 4 B curve d and Figure 4 C).^[11] The multi-level logic gate performs a final XOR logic-gate function which results from the combination

of INH and AND gates (Figure 4 D and Figure S14). Two inputs sets (1,0,1,0) and (1,0,0,1) give a final “1” output, in which the current is recorded as an absolute value independent of the current direction. The XOR logic gate can be used to eliminate inaccurate diagnoses caused by the system malfunctions. High noise components in the sensor signal could spuriously lead to a false “1” readout. However, this output should remain only if In 3 and In 4 are added together for a defective system; it disappears if the system works properly.

The full function of the multi-level logic gate corresponds to an INH–AND–XOR operation. It combines the aptamer-based biochemical logic gate responses of the sensor receptor (INH) with the logic gates of the electrochemical transduction scheme (AND–XOR). By this means a biochemical binding process is transduced into an electrical signal, the sensor signal is enhanced by the ECR effect, and several (bio)chemical input signals are converted into one output signal which reports on the overall status of the system. Different target ranges induce distinguishable and easy to analyze “yes” or “no” outputs, which is of importance in particular for point-of-care diagnostics.

In conclusion, we have successfully established a novel multi-level logic gate based on a sensitive aptamer-binding reaction and the concept of electrochemical rectification, with a final electrical signal output and amplification strategy for logic performance and detection. A rectified charge transport originates from the consecutive charge transfer between the electrode, aptamer-confined surface redox tag, and the redox probes in solution. With ECR as a novel signal amplification strategy, our work offers a sensitive, straightforward, and robust detection technique for aptamer-based electrochemical biosensors. In addition, by carefully considering the concentrations of the ATP and ADA activity unit and integrating the resulting anodic and cathodic current rectifier, we have realized an INH–AND–XOR multi-level logic gate that shows a high switching ratio between output signals “1” and “0” with a final net XOR analysis, which makes it possible to distinguish different health statuses and facilitates fast and accurate diagnosis at the same time. Our sensor may serve as a promising proof of principle that demonstrates increased

computational complexity and enhanced sensor performance by linking multiple logic gates together.

Keywords: aptamers · diagnosis · electrochemical rectification · logic gates · signal amplification

How to cite: *Angew. Chem. Int. Ed.* **2015**, *54*, 7693–7697
Angew. Chem. **2015**, *127*, 7803–7808

- [1] a) X. P. Su, L. M. Smith, *Nucleic Acids Res.* **2004**, *32*, 3115–3123; b) Y. Krishnan, F. C. Simmel, *Angew. Chem. Int. Ed.* **2011**, *50*, 3124–3156; *Angew. Chem.* **2011**, *123*, 3180–3215; c) L. Qian, E. Winfree, J. Bruck, *Nature* **2011**, *475*, 368–372.
- [2] a) F. Wang, X. Liu, I. Willner, *Angew. Chem. Int. Ed.* **2015**, *54*, 1098–1129; *Angew. Chem.* **2015**, *127*, 1112–1114; b) K. Szaciłowski, *Infochemistry*, Wiley, Chichester, **2012**; c) A. P. de Silva, *Molecular Logic-Based Computation*, Royal Society of Chemistry, Cambridge, **2013**; d) *Molecular and Supramolecular Information Processing-From Molecular Switches to Unconventional Computing* (Ed.: E. Katz), Wiley-VCH, Weinheim, **2012**; e) *Bimolecular Computing-From Logic Systems to Smart Sensors and Actuators* (Ed.: E. Katz), Wiley-VCH, Weinheim, 2012; f) M. N. Stojanovic, T. E. Mitchell, D. Stefanovic, *J. Am. Chem. Soc.* **2002**, *124*, 3555–3561; g) J. Elbaz, F. Wang, F. Remacle, I. Willner, *Nano Lett.* **2012**, *12*, 6049–6054; h) T. Li, E. Wang, S. Dong, *J. Am. Chem. Soc.* **2009**, *131*, 15082–15083; i) F. Pu, J. Ren, X. Qu, *Adv. Mater.* **2014**, *26*, 5742–5757.
- [3] a) M. N. Stojanovic, D. Stefanovic, *J. Am. Chem. Soc.* **2003**, *125*, 6673–6676; b) E. Katz, *Curr. Opin. Chem. Biol.* **2015**, *34*, 202–208; c) E. Katz, V. Privman, *Chem. Soc. Rev.* **2010**, *39*, 1835–1857.
- [4] B. M. Frezza, S. L. Cockroft, M. R. Ghadiri, *J. Am. Chem. Soc.* **2007**, *129*, 14875–14879.
- [5] a) Y. Jia, R. Duan, F. Hong, B. Wang, N. Liu, F. Xia, *Soft Matter* **2013**, *9*, 6571–6577; b) D. Kang, R. J. White, F. Xia, X. Zuo, A. Vallee-Belisle, K. W. Plaxco, *NPG Asia Mater.* **2012**, *4*, e1; c) F. Xia, X. Zuo, R. Yang, R. J. White, Y. Xiao, D. Kang, X. Gong, A. A. Lubin, A. Vallée-Bélisle, J. D. Yuen, B. Y. B. Hsu, K. W. Plaxco, *J. Am. Chem. Soc.* **2010**, *132*, 8557–8559.
- [6] A. D. Ellington, J. W. Szostak, *Nature* **1990**, *346*, 818–822.
- [7] a) M. Famulok, G. Mayer, *Acc. Chem. Res.* **2011**, *44*, 1349–1358; b) A. A. Lubin, K. W. Plaxco, *Acc. Chem. Res.* **2010**, *43*, 496–505.
- [8] a) X. Zuo, Y. Xiao, K. W. Plaxco, *J. Am. Chem. Soc.* **2009**, *131*, 6944–6945; b) J. Elbaz, M. Moshe, I. Willner, *Angew. Chem. Int. Ed.* **2009**, *48*, 3834–3837; *Angew. Chem.* **2009**, *121*, 3892–3895; c) Z. Liu, W. Zhang, L. Hu, H. Li, S. Zhu, G. Xu, *Chem. Eur. J.* **2010**, *16*, 13356–13359.
- [9] P. Denisevich, K. W. Willman, R. W. Murray, *J. Am. Chem. Soc.* **1981**, *103*, 4727–4737.
- [10] a) O. Azzaroni, M. Álvarez, A. I. Abou-Kandil, B. Yameen, W. Knoll, *Adv. Funct. Mater.* **2008**, *18*, 3487–3496; b) O. Azzaroni, M. Mir, M. Álvarez, L. Tiefenauer, W. Knoll, *Langmuir* **2008**, *24*, 2878–2883; c) D. Rong, H.-G. Hong, Y. I. Kim, J. S. Krueger, J. E. Mayer, T. E. Mallouk, *Coord. Chem. Rev.* **1990**, *97*, 237–248; d) Y. Liu, A. Offenhäuser, D. Mayer, *Bioelectrochemistry* **2010**, *77*, 89–93.
- [11] a) Y. Liu, A. Offenhäuser, D. Mayer, *Angew. Chem. Int. Ed.* **2010**, *49*, 2595–2598; *Angew. Chem.* **2010**, *122*, 2649–2652; b) Y. Liu, B. Wolfrum, M. Hüske, A. Offenhäuser, E. Wang, D. Mayer, *Angew. Chem. Int. Ed.* **2013**, *52*, 4029–4032; *Angew. Chem.* **2013**, *125*, 4121–4124.
- [12] A. K. Sharma, J. M. Heemstra, *J. Am. Chem. Soc.* **2011**, *133*, 12426–12429.
- [13] H. Urata, K. Nomura, S.-i. Wada, M. Akagi, *Biochem. Biophys. Res. Commun.* **2007**, *360*, 459–463.
- [14] a) R. J. White, N. Phares, A. A. Lubin, Y. Xiao, K. W. Plaxco, *Langmuir* **2008**, *24*, 10513–10518; b) S. J. P. Canete, W. Yang, R. Y. Lai, *Chem. Commun.* **2009**, 4835–4837.
- [15] a) R. Nutiu, J. M. Y. Yu, Y. Li, *ChemBioChem* **2004**, *5*, 1139–1144; b) L. Feng, Z. Zhang, J. Ren, X. Qu, *Biosens. Bioelectron.* **2014**, *62*, 52–58.
- [16] J. J. Sanchez, G. Monaghan, C. Børsting, G. Norbury, N. Morling, H. B. Gaspar, *Ann. Hum. Genet.* **2007**, *71*, 336–347.
- [17] X.-J. Xing, X.-G. Liu, H. Yue, Q.-Y. Luo, H.-W. Tang, D.-W. Pang, *Biosens. Bioelectron.* **2012**, *37*, 61–67.
- [18] a) M. W. Gorman, E. O. Feigl, C. W. Buffington, *Clin. Chem.* **2007**, *53*, 318–325; b) M. F. Baganha, A. Pêgo, M. A. Lima, E. V. Gaspar, A. R. Cordeiro, *Chest* **1990**, *97*, 605–610.
- [19] a) H. Li, D. Li, J. Liu, Y. Qin, J. Ren, S. Xu, Y. Liu, D. Mayer, E. Wang, *Chem. Commun.* **2012**, *48*, 2594–2596; b) L. Feng, A. Sivanesan, Z. Lyu, A. Offenhäuser, D. Mayer, *Biosens. Bioelectron.* **2015**, *66*, 62–68.
- [20] J. Zhang, L. Wang, D. Pan, S. Song, C. Fan, *Chem. Commun.* **2007**, 1154–1156.
- [21] a) E. J. Cho, L. Yang, M. Levy, A. D. Ellington, *J. Am. Chem. Soc.* **2005**, *127*, 2022–2023; b) K. Hsieh, Y. Xiao, H. T. Soh, *Langmuir* **2010**, *26*, 10392–10396; c) X. Chen, L. Ge, B. Guo, M. Yan, N. Hao, L. Xu, *Biosens. Bioelectron.* **2014**, *58*, 48–56; d) K.-J. Huang, Y.-J. Liu, H.-B. Wang, Y.-Y. Wang, Y.-M. Liu, *Biosens. Bioelectron.* **2014**, *55*, 195–202; e) I. Palchetti, M. Mascini, *Anal. Bioanal. Chem.* **2012**, *402*, 3103–3114.
- [22] a) M. S. Coleman, J. Donofrio, J. J. Hutton, L. Hahn, *J. Biol. Chem.* **1978**, *253*, 1619–1626; b) H. A. Simmonds, R. J. Levinsky, D. Perrett, D. R. Webster, *Biochem. Pharmacol.* **1982**, *31*, 947–951.

Received: March 12, 2015

Published online: May 8, 2015